arXiv:cond-mat/0202367v2 [cond-mat.mes-hall] 12 Jun 2002

Even-odd parity effects in conductance and shot noise of metal-atomic wire-metal(superconducting) junctions

Tae-Suk Kim[1,2,3] and S. Hershfield[3]
[1] *Institute of Physics and Applied Physics, Yonsei University, Seoul 120-749, Korea*
[2] *School of Physics, Korea Institute for Advanced Study, Seoul 130-012, Korea*
[3] *Department of Physics, University of Florida, Gainesville FL 32611-8440*

(Dated: February 1, 2008)

In this paper, we study the conductance and shot noise in transport through a multi-site system in a two terminal configuration. The dependence of the transport on the number of atoms in the atomic wire is investigated using a tight-binding Hamiltonian and the nonequilibrium Green's function method. In addition to reproducing the even-odd behavior in the transmission probability at the Fermi energy or the linear response conductance in the normal-atomic wire-normal metallic(NAN) junctions, we find the following: (i) The shot noise is larger in the even-numbered atomic wire than in the odd-numbered wire. (ii) The Andreev conductance displays the same even-odd parity effects in the normal-atomic wire-superconducting(NAS) junctions. In general, the conductance is higher in the odd-numbered atomic wire than in the even-numbered wire. When the number of sites (N) is odd and the atomic wire is mirror symmetric with respect to the center of the atomic wire, the conductance does not depend on the details of the hopping matrices in the atomic wire, but is solely determined by the coupling strength to the two leads. When N is even, the conductance is sensitive to the values of the hopping matrices.

PACS numbers: 73.63.Nm, 74.50.+r

I. INTRODUCTION

Electron transport through an atomic wire is realized in scanning tunneling microscope(STM) experiments[1,2] and break junctions[3]. An array of quantum dots[4] can be considered as an artificial atomic wire. In the STM experiments, a true atomic wire was realized as the dipped gold STM tip is slowly retracted from the Au substrate. Just before breaking, the metallic contacts become thinner down to one atom wide and consisting of a few bridging atoms. Yanson and others[1] succeeded in forming chains of gold atoms up to seven atoms long. The observed conductance[1,2,5] stayed close to one unit of the conductance quantum before breaking.

A quantum dot is a collection of electrons within a small space and can be considered as an artificial atom. Since electrons are confined to the small region, electrons experience the strong Coulomb repulsion and their energy level spectrum is discrete. Like electrons in atoms, the charge and spin of electrons are quantized in quantum dots. In contrast to the atoms in the periodic table, it is easy to control the energy level spacing, the strength of Coulomb interaction, the number of electrons (charge), spin, etc in quantum dots. When quantum dots are arranged as a linear chain, the system can be considered as an "atomic" wire. Some I-V curves have been measured in an array of quantum dots. The splitting of the Coulomb peaks[4] was observed in the conductance when the interdot tunneling rate is strong compared with the coupling to external electrodes.

In this paper, we study the conductance and shot noise in transport through an atomic wire in a two termial configuration. The atomic wire in our study consists of the monovalent atoms like Na, Au, Ag, Cu, etc. and is modeled by a single orbital tight-binding Hamiltonian(see Fig. 1.) When two metallic leads, connected to the atomic wire, are both normal, we study the dependence of linear response conductance and shot noise on the number of atoms in the atomic chain. When one lead is normal and the other is superconducting, the dependence of the Andreev conductance on the number of atoms in the chain is studied. Our discussion is confined to the linear response regime or to the case of weak source-drain bias voltage.

The even-odd behavior of the linear response conductance or oscillation of the conductance as a function of the number of atoms in the atomic wire was theoretically studied using *ab initio* calculations[6,7]. In heterogeneous carbon atomic wires[6] where the carbon atomic wires are connected to two metal electrodes, the linear response conductance is found to be oscillating as a function of the number of C atoms in the atomic wire. The conductance is smaller than the conductance quantum $G_Q = 2e^2/h$ and is higher in the odd-numbered atomic wires than in the even-numbered systems. On the other hand, the conductance is very close to G_Q in the homogeneous sodium atomic wire[7] when the number of atoms in the wire is odd. In general, the conductance is higher for the atomic wire with an odd number of atoms than with an even number of atoms. This even-odd parity effect in the conductance can be understood based upon the tight-binding Hamiltonian[8,9] for the atomic wire. In addition to reproducing the even-odd behavior of the conductance in the metal-atomic wire-metal junction, we also find the same oscillation in the Andreev conductance as a function of the number of atoms in the atomic wire for the metal-atomic wire-superconducting junctions. When the number of sites (N) is odd and the atomic wire is mirror symmetric with respect to the center of the atomic wire, the conductance does not depend on the details of the hopping matrices in the atomic wire, but is solely determined by the coupling strength to the two leads. When N is even, the conductance is sensitive to the values of the hopping matrices.

In recent STM experiments of gold nanocontacts[5], a small variation of conductance within the region of a unit conductance quantum was observed (Fig. 1a of reference[5]) as the STM tip is stretched before breaking. Since the conductance is close to the unit conductance quantum, the gold chain is one atom thick. A small variation but abrupt jump in the conductance might originate from an addition of an extra gold atom to the chain. That is, the observed conductance variation may be a signature of the even-odd parity effects in the atomic wire.

This paper is organized as follows. In Sec. II, we study the transport through multi-sites which are connected to the two normal metallic leads. We consider the normal-superconducting junctions passing through the multi-sites in Sec. III. Two sections are the separate works and can be read independently. Our study is summarized in Sec. IV.

II. NORMAL-NORMAL METALLIC(N-N) JUNCTIONS CONNECTED BY MULTI-SITES

In this section we study the current and its noise in the transport through multi-resonant sites in a two-terminal configuration where two leads are in the normal metallic state. The formalism is most conveniently simplified using the matrix notations. The current is given in a well-known Landauer-Büttiker form[10,11] and the shot noise is also expressed in the familiar binomial form[12] except for some special cases.

Applying the formalism to the serial multi-site system or the atomic wire connected to two metallic leads, we give a simple explanation of the even-odd behavior in the transmission probability at the Fermi energy or linear response conductance which was reported in the recent theoretical works[6,7]. In a mirror symmetric atomic wire, the transmission probability at the Fermi energy takes the same value which depends only on the coupling strength to the two leads, when the number of sites is odd. On the other hand, for the system with an even number of sites, the transmission probability depends on the detailed values of the hopping matrices between neighboring sites. This even-odd behavior can be understood in terms of the level-splitting in quantum physics and the particle-hole symmetry in the energy spectrum when all the energy levels of atoms lie at the Fermi energy. We also find that the shot noise in the transport through multi-site system is oscillating as a function of the number of atoms in the atomic wire.

The multi-site system made of monovalent atoms (Na, Au, Ag, Cu) can be described by the model Hamiltonian,

$$\begin{aligned} H_{cb} &= \sum_{p=L,R}\sum_k \epsilon_{pk} c^\dagger_{pk} c_{pk}, & (2.1)\\ H_d &= \sum_{i=1}^{N} E_i d_i^\dagger d_i + \sum_{i\neq j} W_{ij} d_i^\dagger d_j, & (2.2)\\ H_1 &= \sum_{pk}\sum_i \left[V_{pi} c^\dagger_{pk} d_i + V_{ip} d_i^\dagger c_{pk}\right]. & (2.3)\end{aligned}$$

Since the electron spin does not play any role in the N-N junctions, the spin index will be suppressed in this section. Electrons can flow from one lead to the other one through all the sites when a finite source-drain voltage is applied. All the sites are connected to each other via tunneling. The serial multi-site model is recovered when $W_{ij} = 0$ unless $j = i \pm 1$ and $V_{iL} = V_L \delta_{i,1}$ and $V_{iR} = V_R \delta_{i,N}$. The algebra is most conveniently simplified and becomes compact when the Hamiltonian is written in a matrix form by introducing

$$\begin{aligned} \Psi_d^\dagger &= \begin{pmatrix} d_1^\dagger & d_2^\dagger & \cdots & d_N^\dagger \end{pmatrix}, & (2.4)\\ V_p^\dagger &= \begin{pmatrix} V_{p1} & V_{p2} & \cdots & V_{pN} \end{pmatrix}, & (2.5)\end{aligned}$$

and $H_{d,ii} = E_i, H_{d,ij} = W_{ij}$. With these notations, the model Hamiltonian becomes

$$\begin{aligned} H_d &= \Psi_d^\dagger H_d \Phi_d, & (2.6)\\ H_1 &= \sum_{pk}\left[c^\dagger_{pk} V_p^\dagger \Psi_d^\dagger + \Psi_d^\dagger V_p c_{pk}\right]. & (2.7)\end{aligned}$$

A. Current and shot noise

The current operator which is defined as the variation per unit time of electron charges in the left or right lead can be written in a matrix form as

$$\hat{I}_p = \frac{e}{i\hbar}[\hat{N}_p, H] = \frac{e}{i\hbar}\sum_k \left[c^\dagger_{pk} V_p^\dagger \Psi_d - \Psi_d^\dagger V_p c_{pk}\right] \quad (2.8)$$

After thermal averaging the current operator, current is written in terms of the mixed Green's function out of equilibrium.

$$\begin{aligned} I_p &= 2e\sum_k \mathrm{Im}\mathrm{Tr} G^<_{dp}(t,kt) V_p^\dagger, & (2.9)\\ i\hbar G_{dp}(t,kt') &= \langle T_c \Psi_d(t) c^\dagger_{pk}(t')\rangle. & (2.10)\end{aligned}$$

Here T_c means contour-ordering where the contour encloses the real-time axis[13,14]. Using the Dyson equation for the mixed Green's function G_{dp} and the Green's functions of two leads, the above expression of current is reduced to a simple compact Landauer-Büttiker form[10,11].

$$\begin{aligned} I_L &= \frac{2e}{h}\int d\epsilon\; T(\epsilon)[f_R(\epsilon) - f_L(\epsilon)], & (2.11)\\ T(\epsilon) &= 4\mathrm{Re}\mathrm{Tr}[\Gamma_L D^r(\epsilon)\Gamma_R D^a(\epsilon)]. & (2.12)\end{aligned}$$

The factor 2 is recovered in I_L to take into account two directions of an electron spin. $\Gamma_p = \pi N_p V_p V_p^\dagger (p = L, R)$ is the linewidth matrix. $D^{r,a}$ is the retarded (advanced) part of Green's function of the multi-site system which is defined by

$$i\hbar D(t,t') \;=\; \langle T_c \Psi_d(t) \Psi_d^\dagger(t') \rangle. \tag{2.13}$$

$f_p (p = L, R)$ is the Fermi-Dirac thermal distribution function in the left and right leads.

The current noise is defined as the current-current correlation function.

$$S(t,t') \;=\; \langle \delta\hat{I}(t)\delta\hat{I}(t')\rangle + \langle \delta\hat{I}(t')\delta\hat{I}(t)\rangle. \tag{2.14}$$

Here $\delta\hat{I}(t) = \hat{I}(t) - \langle \hat{I}(t) \rangle$ is the current fluctuation operator. To compute the current noise, we introduce the current Green's function,

$$i\hbar G_{II}(t,t') \;=\; \langle T_c \delta\hat{I}(t)\delta\hat{I}(t')\rangle. \tag{2.15}$$

Using the greater and lesser current Green's functions, $G_{II}^{>}(t,t') = \langle \delta\hat{I}(t)\delta\hat{I}(t')\rangle$ and $G_{II}^{<}(t,t') = -\langle \delta\hat{I}(t')\delta\hat{I}(t)\rangle$, the current noise can be written as

$$S(t,t') \;=\; \hbar G_{II}^{>}(t,t') - \hbar G_{II}^{<}(t',t). \tag{2.16}$$

Since $G_{II}^{>}(t,t') = -G_{II}^{<}(t',t)$, calculation of only the lesser current Green's function is needed to find the current noise. For the noninteracting electrons in the multi-site system, there are only six Feynman diagrams, as shown in Fig. 2, contributing to the current noise. Detailed calculations of each diagram are described in the Appendix A. The current noise expression is given by the equation,

$$\begin{aligned} S_0 \;&=\; \frac{4e^2}{h}\int d\epsilon [f_L \bar{f}_L + f_R \bar{f}_R] \mathrm{Tr}\mathbf{T}^2 \\ &+ \frac{4e^2}{h}\int d\epsilon [f_L \bar{f}_R + \bar{f}_L f_R] \left[\mathrm{Tr}\mathbf{T} - \mathrm{Tr}\mathbf{T}^2\right] \end{aligned} \tag{2.17}$$

Additional factor 2 is multiplied to get the spinful result of S_0. Here $\mathbf{T} = 4\Gamma_L D^r \Gamma_R D^a$ and $f_p (p = L, R)$ is the Fermi-Dirac thermal function in the left and right electrodes and $\bar{f}_p = 1 - f_p$. As expected, the current noise S_0 is symmetrical in the lead indices L and R. In the expression of current, the transmission probability $T(\epsilon)$ is defined as $T(\epsilon) = \mathrm{Tr}\mathbf{T}$. Manipulating the thermal functions, we can rewrite the expression of S_0 as

$$\begin{aligned} S_0 \;&=\; \frac{4e^2}{h}\int d\epsilon [f_L \bar{f}_L + f_R \bar{f}_R] T(\epsilon) \\ &+ \frac{4e^2}{h}\int d\epsilon [f_L - f_R]^2 \mathrm{Tr}\left\{\mathbf{T}(\epsilon) - [\mathbf{T}(\epsilon)]^2\right\} \end{aligned} \tag{2.18}$$

The first line is the thermal or Johnson noise and remains finite at nonzero temperature. The second line is nonzero only out of equilibrium and is the so-called shot noise deriving from the discreteness of electron's charge. We note that the integrand in the second line is simplified to the familiar binomial expression[12] $T(\epsilon)[1 - T(\epsilon)]$ except when both $\det\Gamma_L \neq 0$ and $\det\Gamma_R \neq 0$. This point can be easily proved by noting that $\mathbf{T}$ and $\mathbf{T}^2$ can be diagonalized at the same time and the trace is a sum of diagonal elements. Only one diagonal element is non-zero after diagonalization and all the others are zero. As concrete examples, the familiar binomial expression of S_0 is obtained for the two-site or the serial multi-site systems. Note that for a 2×2 matrix A we have the identity

$$\mathrm{Tr}A^2 \;=\; [\mathrm{Tr}A]^2 - 2\det A. \tag{2.19}$$

However, $\det\mathbf{T} = 0$ since $\det\Gamma_L = 0 = \det\Gamma_R$. That is, the current noise for the two-site system is reduced to the familiar binomial expression. There are exceptional cases[15] of two-site system for which $\det\Gamma_L \neq 0 \neq \det\Gamma_R$. In this case, the familiar binomial expression of the shot noise is not recovered.

B. Atomic wire: serial multi-sites

In this section, we apply the formalism of the previous section to the metal-atomic wire-metal junctions for which the atomic wire is modeled by the tight-binding Hamiltonian. In a serial configuration of multi-sites, the hopping matrices are non-zero only between two neighboring sites,

$$W_{ij} \;=\; t_i \delta_{i+1,j} + t_j^* \delta_{i,j+1}. \tag{2.20}$$

Since only the left (right)-most site is connected to the left (right) lead, the linewidth matrices are simplified as

$$\Gamma_{L,ij} \;=\; \Gamma_L \;\delta_{i,1}\delta_{j,1}, \tag{2.21}$$

$$\Gamma_{R,ij} \;=\; \Gamma_R \;\delta_{i,N}\delta_{j,N}. \tag{2.22}$$

Under this condition, the transmission probability is given by the expression,

$$T(\epsilon) \;=\; 4\mathrm{Tr}\Gamma_L D^r \Gamma_R D^a = 4\Gamma_L \Gamma_R \;|D_{1N}^r(\epsilon)|^2. \tag{2.23}$$

Here D_{1N}^r is the retarded part of the Green's function defined by

$$i\hbar D_{1N}(t,t') \;=\; \langle T_c d_1(t) d_N^\dagger(t') \rangle, \tag{2.24}$$

and is given by the $(1, N)$ element of $D^r(\epsilon) = [\epsilon - H_d + i\Gamma]^{-1}$. Here $\Gamma = \Gamma_L + \Gamma_R$ is the total linewidth matrix. Using the cofactor of the matrix, we find D_{1N}^r,

$$\begin{aligned} D_{1N}^r(\epsilon) \;&=\; [\epsilon - H_d + i\Gamma]_{1N}^{-1} \\ &=\; \frac{t_1 t_2 \cdots t_{N-1}}{Z_N(\epsilon)}, \end{aligned} \tag{2.25}$$

$$Z_N(\epsilon) \;=\; \det[\epsilon - H_d + i\Gamma]. \tag{2.26}$$

The determinant Z_N is calculated iteratively.

Consider the case of $E_i = 0$ for all $i = 1, 2, \cdots, N$ and calculate the transmission probability at the Fermi energy. This particle-hole symmetric energy structure seems to be realized in the *ab initio* calculation of the homogeneous sodium atomic wire[7]. Depending on the parity of the number of sites, the determinant takes on different forms,

$$\begin{aligned} Z_{2N}(0) &= (-1)^N\Gamma_L\Gamma_R|t_2t_4\cdots t_{2N-2}|^2 \\ &\quad +(-1)^N|t_1t_3\cdots t_{2N-1}|^2, \qquad (2.27) \\ Z_{2N+1}(0) &= i(-1)^N\Gamma_R|t_1t_3\cdots t_{2N-1}|^2 \\ &\quad +i(-1)^N\Gamma_L|t_2t_4\cdots t_{2N}|^2. \qquad (2.28) \end{aligned}$$

Accordingly, the transmission probability has the even-odd parity dependence:

$$\begin{aligned} T_{2N}(0) &= \frac{4\Gamma_L\Gamma_R|t_1t_2\cdots t_{2N-1}|^2}{[\Gamma_L\Gamma_R|t_2t_4\cdots t_{2N-2}|^2+|t_1t_3\cdots t_{2N-1}|^2]^2}, \qquad (2.29) \\ T_2(0) &= \frac{4\Gamma_L\Gamma_R|t_1|^2}{[\Gamma_L\Gamma_R+|t_1|^2]^2}, \qquad (2.30) \end{aligned}$$

and

$$\begin{aligned} T_{2N+1}(0) &= \frac{4\Gamma_L\Gamma_R|t_1t_2\cdots t_{2N}|^2}{[\Gamma_L|t_2t_4\cdots t_{2N}|^2+\Gamma_R|t_1t_3\cdots t_{2N-1}|^2]^2}, \qquad (2.31) \\ T_1(0) &= \frac{4\Gamma_L\Gamma_R}{[\Gamma_L+\Gamma_R]^2}. \qquad (2.32) \end{aligned}$$

The conditions of perfect transmission can be readily found from the above equations.

When the hopping matrices are mirror symmetric with respect to the the center of the atomic wire, the above expression of $T_N(0)$ for odd N is further simplified.

$$T_{2N+1}(0) = \frac{4\Gamma_L\Gamma_R}{[\Gamma_L+\Gamma_R]^2}. \qquad (2.33)$$

Note that this value does not depend on the detailed values of the hopping matrices between neighboring sites. On the other hand, the transmission probability $T_N(0)$ for even N depends on the detailed values of hopping matrices.

When the hopping matrices between neighboring sites are all equal, $t_i = t$ for all i's, the transmission probability $T_N(0)$ is further simplified to

$$\begin{aligned} T_{2N}(0) &= \frac{4\Gamma_L\Gamma_R t^2}{[t^2+\Gamma_L\Gamma_R]^2}, \qquad (2.34) \\ T_{2N+1}(0) &= \frac{4\Gamma_L\Gamma_R}{[\Gamma_L+\Gamma_R]^2}. \qquad (2.35) \end{aligned}$$

The transmission probability at the Fermi energy in the even-numbered atomic wire still depends on the hopping matrix. Perfect transmission is achieved when $\Gamma_L = \Gamma_R$ in the odd-numbered atomic wire, and when $t^2 = \Gamma_L\Gamma_R$ in the even-numbered atomic wire.

The even-odd parity behavior of the transmission probability at the Fermi energy is a consequence of the energy level splitting in quantum physics and the particle-hole symmetry of atomic energy levels. In the particle-hole symmetric case, all the atomic energy levels lie at the Fermi energy ($E_i = 0$) when the hopping between atoms and the coupling to the leads are turned off. When hopping between neighboring atoms in the atomic wire is turned on, the degeneracy in atomic energy levels is lifted and the energy level structure still keeps the particle-hole symmetry (see the Appendix B.) Note that the values of t_i's have no influence on the particle-hole symmetry of split atomic energy levels.

In the odd-numbered atomic wire, one level always lies at the Fermi energy and all others are distributed symmetrically with respect to the Fermi energy(E_F). Note that $Z_{2N+1}(0)$ is equal to 0 when $\Gamma_{L,R} = 0$. This vanishing determinant means that at least one energy level lies at E_F. Since no degeneracy remains in the presence of hopping between atomic sites, only one level is located at the Fermi energy. When the coupling to external leads is turned on, the discrete energy levels become broadened. The transmission probability $T_N(\epsilon)$ for odd N is always peaked at $\epsilon = 0$ or the Fermi energy.

On the other hand, all energy levels are distributed symmetrically with respect to the Fermi energy without any level at E_F for the even-numbered atomic wires. Since $Z_{2N}(0)$ is not equal to 0 when $\Gamma_{L,R} = 0$, the degeneracy-lifted atomic energy levels cannot lie at the Fermi energy in the even-numbered atomic wire. Though no energy level is present at the Fermi energy for the even-numbered atomic wire, either a dip or a peak in $T_N(\epsilon)$ for even N is possible at the Fermi energy $\epsilon = 0$ when $\Gamma_{L,R} \neq 0$, depending on the relative magnitudes of the hopping integral (level-splitting) in the atomic wire and the coupling strength (linewidth) to the leads. When $t_i = t$ for all i's and $\Gamma_L = \Gamma_R$, the transmission probability is dipped(peaked) at the Fermi energy($\epsilon = 0$) when $t > (\leq)\Gamma_{L,R}$, respectively.

To illustrate the even-odd parity dependence of the transmission probability, $T_N(\epsilon)$ is displayed in Fig. 3 for differing N's (the number of atoms in the atomic wire). To reproduce the results of the *ab initio* calculations[6,7], model parameters are chosen such that $E_i = 0$ for all sites and all tight-binding hopping matrices are equal, $t_i = t$. For typical metals, t is of the order of 1eV. Furthermore, the bonding in the gold atomic wire is almost two times stronger than in the bulk[5]. To simulate the homogeneous monovalent atomic wires (Au, Na, Ag, Cu), we take some intermediate value of $\Gamma_{L,R}/t = 0.7$ in Fig. 3. It is a reasonable approximation to assume that the bonding between the atom in the atomic wire and the atom in the leads is intermediate compared to the bonding in the chain or in the bulk. Clearly, $T(\epsilon)$ is peaked at the Fermi energy in the odd-numbered atomic wires and is suppressed at $\epsilon = 0$ in the even-numbered atomic wires. The number of peaks in $T(\epsilon)$ agrees with the number of atoms in the atomic wire.

Sharp asperity at the STP tip seems to be necessary for the conductance quantization according to recent numerical works[16]. In our approach, the blunt STM tip can be simulated by increasing the coupling strength between the electrodes and the atomic wire. Note that the left (right)-most atom in the chain is coupled to more atoms in the leads for blunt tips than for sharp tips. The results for $\Gamma_{L,R}/t = 1.2$ are displayed in Fig. 4. Though the spectral shape of $T_N(\epsilon)$ is broadened compared to Fig. 3, the even-odd parity effects persist in this case, too. Note that the dip of $T_{2N}(\epsilon)$ at the Fermi energy for $t > \Gamma_{L,R}$ is transformed into a peak when $t \leq \Gamma_{L,R}$.

In the heterogeneous carbon atomic wires[6], charge transfer occurs from the metallic electrode into the carbon chain, and a Schottky-like barrier is formed between the electrodes and the carbon chain. Due to the Schottky-like barrier, the coupling strength between the electrodes and the chain is weaker than in the homogeneous systems. The authors suggest that the reduced transmission probability, $T(0) < 1$, is a result of the higher barrier between the chain and the leads. Higher barrier or weaker coupling leads to sharper line shape in the transmission probability. We would like to propose a different interpretation. As long as the couplings to two electrodes are symmetrical and all the hopping matrices are the same, the broken particle-hole symmetry in the energy levels of atoms in the chain can be the reason for the reduced $T(0) < 1$. The doped excess charge is not distributed uniformly over C atoms in the chain[6]. The assumption of $E_i = 0$ for all atomic sites seems to be violated. According to the Friedel sum rule[17], excess (depleted) charges will shift downward (upward) the energy levels E_i of atoms in the chain. Broken particle-hole symmetry in the energy structure leads to reduced transmission probability at the Fermi energy in the tight-binding Hamiltonian approach.

We can also study the effects of disorder in the hopping matrices in the atomic wire on the transmission probability. While retracting the STM tip from the sample, atomic rearrangements occur according to molecular dynamics simulations[5]. Some randomness in the bonding between neighboring atoms might be present. To simulate this situation, we introduce the disorder in the magnitude of t's such that $t_i = t(1+\delta_i)$ with some randomness δ_i. Typical results of $T(\epsilon)$ with disordered t_i's with $|\delta_i| \leq 0.2$ are displayed in Fig. 5. Even in the presence of disorder in the hopping matrices, the even-odd parity behavior may persist as far as the disorder is not strong and the coupling to the leads is not close to the values of hopping matrices.

We predict that the shot noise also displays the even-odd behavior depending on the number of atoms in the atomic wire. First note that $\mathrm{Tr}\mathbf{T}^2 = [T(\epsilon)]^2$ due to the simple structure of the linewidth matrices. Hence the shot noise is given by the familiar binomial expression[12] and at zero temperature by

$$S_0 = \frac{4e^2}{h}\int_{\mu_R}^{\mu_L} d\epsilon\; T(\epsilon)[1 - T(\epsilon)]. \qquad (2.36)$$

When the source-drain bias voltage is small such that the transmission probability does not change much over the energy $eV = \mu_L - \mu_R$ near the Fermi energy, the shot noise can be approximated as $S_0 = (4e^2/h)T(0)[1 - T(0)]eV$. In the homogeneous sodium atomic wire[7], the transmission probability was found to be very close to unity when the number of atoms is odd. On the other hand, the transmission probability is smaller than unity when the number of atoms is even. We conclude that the shot noise at low source-drain bias voltages is larger in the even-numbered atomic wires than in the odd-numbered atomic wires.

III. NORMAL-SUPERCONDUCTING JUNCTIONS CONNECTED BY MULTI-SITES

In this section, we study the I-V curves in the normal-superconducting(N-S) junctions connected by multi-sites in between. The left lead is a normal metal and the right lead is assumed to be the simple BCS s-wave superconductors with the constant energy gap. In our simple approach, the energy gap in the superconducting lead is assumed to be constant and not degraded near the junction by the atomic wire. Local density of states (DOS) at the atomic sites is modified by the superconducting energy gap of the right lead and its structure depends on the parity in the number of atoms in the atomic wire. In addition, the DOS structure takes different shapes depending on the atom's position in the chain. As in the N-N junctions connected by an atomic wire, the Andreev conductance shows the even-odd parity behavior.

To describe the superconducting state, it is convenient to use the Nambu spinor notation. The two leads are described by the Hamiltonian,

$$\begin{aligned} H_{cb} &= \sum_{p=L,R}\sum_{k} \Psi^{\dagger}_{pk} E_{pk} \Psi_{pk}, && (3.1)\\ E_{Lk} &= \begin{pmatrix} \epsilon_{Lk} & 0 \\ 0 & -\epsilon_{Lk} \end{pmatrix}, \quad E_{Rk} = \begin{pmatrix} \epsilon_{Rk} & \Delta_R \\ \Delta^*_R & -\epsilon_{Rk} \end{pmatrix}, && (3.2)\\ \Psi_{pk} &= \begin{pmatrix} c_{pk\uparrow} \\ c^{\dagger}_{p-k\downarrow} \end{pmatrix}. && (3.3) \end{aligned}$$

Here ϵ_{pk} is the energy dispersion in the left ($p = L$) and right ($p = R$) leads and Δ_R is the energy gap in the right superconducting lead. Since the phase of the energy gap Δ_R in the N-S junction does not play any role, Δ_R is taken to be real. The Hamiltonian of the multi-sites is also written using the Nambu spinor notation as

$$\begin{aligned} H_d &= \sum_i \Psi^{\dagger}_{di} \begin{pmatrix} E_i & 0 \\ 0 & -E_i \end{pmatrix} \Psi_{di} \\ &\quad + \sum_{i\neq j} \Psi^{\dagger}_{di} \begin{pmatrix} W_{ij} & 0 \\ 0 & -W^*_{ij} \end{pmatrix} \Psi_{dj}, \qquad (3.4) \end{aligned}$$

where $\Psi^{\dagger}_{di} = \begin{pmatrix} d^{\dagger}_{i\uparrow} & d_{i\downarrow} \end{pmatrix}$. E_i is the energy level of the i-th site and W_{ij} is the hopping matrix between two sites i and j. The coupling between two leads and the multi-sites is described by the tunneling Hamiltonian,

$$H_1 \;=\; \sum_{pki}\left[\Psi^\dagger_{pk}\begin{pmatrix}V_{pi} & 0\\ 0 & -V_{ip}\end{pmatrix}\Psi_{di} + H.c.\right]. \tag{3.5}$$

Using this model Hamiltonian, we study the Andreev reflection[18] in the N-S junction.

A. Multi site: General formalism

The algebra is highly simplified when the Hamiltonian of the multi-site system is written in terms of the matrix. Introducing new notations

$$V^\dagger_p \;\equiv\; \begin{pmatrix}V_{p1} & 0 & V_{p2} & 0 & \cdots & V_{pN} & 0\\ 0 & V_{1p} & 0 & V_{2p} & \cdots & 0 & V_{Np}\end{pmatrix}, \tag{3.6}$$

$$\mathbf{H}_{d,ii} \;=\; \begin{pmatrix}E_i & 0\\ 0 & -E_i\end{pmatrix}, \quad \mathbf{H}_{d,ij} \;=\; \begin{pmatrix}W_{ij} & 0\\ 0 & -W_{ji}\end{pmatrix}, \tag{3.7}$$

$$\Psi^\dagger_d \;=\; \left(\Psi^\dagger_{d1}\;\;\Psi^\dagger_{d2}\;\;\cdots\Psi^\dagger_{dN}\right), \tag{3.8}$$

the model Hamiltonian can be written as

$$H_d \;=\; \Psi^\dagger_d H_d \Psi_d, \tag{3.9}$$

$$H_1 \;=\; \sum_{pk}\left[\Psi^\dagger_{pk}\tau_3 V^\dagger_p \Psi_d + \Psi^\dagger_d V_p \tau_3 \Psi_{pk}\right]. \tag{3.10}$$

Here τ_3 is the third component of the Pauli matrices. The current operator can be also written in a simple compact form using the new notation,

$$\hat{I}_p \;=\; \frac{e}{i\hbar}\sum_k\left[\Psi^\dagger_{pk}V^\dagger_p\Psi_d - H.c.\right]. \tag{3.11}$$

The thermally averaged current is then

$$I_p \;=\; 2e\sum_k \mathrm{ImTr}V^\dagger_p G^<_{dp}(t,kt). \tag{3.12}$$

The mixed Green's function is defined and determined by the Dyson equation,

$$G_{dp}(t,kt') \;=\; \frac{1}{i\hbar}\langle T_c\Psi_d(t)\Psi^\dagger_{pk}(t')\rangle$$

$$\;=\; \int_C dt_1\; D(t,t_1)V_p\tau_3 G_{cp}(k;t_1,t') \tag{3.13}$$

$$i\hbar D(t,t') \;=\; \langle T_c\Psi_d(t)\Psi^\dagger_d(t')\rangle. \tag{3.14}$$

Inserting all the relevant Green's functions of two leads, the current can be expressed as

$$I_L \;=\; \frac{4e}{h}\int d\epsilon \mathrm{Tr}\left[D^r\cdot\pi N_L V_L\hat{f}_L V^\dagger_L\cdot D^a\cdot\pi N_L V_L\tau_3 V^\dagger_L - D^r\cdot\pi N_L V_L\tau_3\hat{f}_L V^\dagger_L\cdot D^a\cdot\pi N_L V_L V^\dagger_L\right]$$

$$+\frac{4e}{h}\int d\epsilon \mathrm{Tr}\pi N_R g_2(\epsilon)V_R\tau_3\hat{\Omega}_R\tau_3 V^\dagger_R\left[D^r\cdot\pi N_L V_L\tau_3\hat{f}_L V^\dagger_L\cdot D^a - D^a\cdot\pi N_L V_L\tau_3 f(\epsilon)V^\dagger_L D^r\right]. \tag{3.15}$$

This equation of current is our starting point for the study of the even-odd parity behavior in the Andreev conductance in the metal-atomic wire-superconducting junctions. $D^{r,a}$ is the retarded (advanced) part of the Green's function of the multi-site system. Note that $D^a = [D^r]^\dagger$. Other notations are listed below.

$$\hat{f}_L(\epsilon) \;=\; \begin{pmatrix}f(\epsilon-\mu_L) & 0\\ 0 & f(\epsilon+\mu_L)\end{pmatrix}, \tag{3.16}$$

$$\hat{\Omega}_R \;=\; \begin{pmatrix}\epsilon & \Delta_R\\ \Delta^*_R & \epsilon\end{pmatrix}, \tag{3.17}$$

$$g(\epsilon) \;=\; \int\frac{d\epsilon_k}{\pi}\frac{1}{(\epsilon+i\delta)^2-\epsilon_k^2-|\Delta_R|^2}$$

$$\;=\; -\left[\frac{\theta(\Delta_R-|\epsilon|)}{\sqrt{\Delta_R^2-\epsilon^2}} + i\mathrm{sgn}(\epsilon)\frac{\theta(|\epsilon|-\Delta_R)}{\sqrt{\epsilon^2-\Delta_R^2}}\right] \tag{3.18}$$

The second line in g is obtained in a wide conduction band limit. We write $g = g_1 + ig_2$. Note that g is real for $|\epsilon| < \Delta_R$ and imaginary for $|\epsilon| > \Delta_R$. To simplify the algebra, the bias voltages are chosen as $\mu_L = eV$ and $\mu_R = 0$. The first line in Eq. (3.15) is a contribution from the Andreev reflection[18]. The integrand in the first line remains finite over the entire energy range, though it is appreciable inside the gap. The electron incident from the normal metallic lead forms a Cooper pair with its partner, tunnels into the superconducting lead and leave a hole in the normal metallic lead. This remaining hole moves along the time-reversed track of the incident electron. Note that $g_2(\epsilon) = 0$ for $|\epsilon| < \Delta_R$. That is, the second line in Eq. (3.15) is the contribution from quasiparticles excited over the superconducting energy gap. The above expression of current can be applied to any configuration of multiple resonant sites connected to the two leads.

B. One site

To begin we consider the N-S junction connected by the one-site system. The coupling matrices to the leads are

$$V_L^\dagger = \begin{pmatrix} V_{L1} & 0 \\ 0 & V_{1L} \end{pmatrix}, \quad V_R^\dagger = \begin{pmatrix} V_{R1} & 0 \\ 0 & V_{1R} \end{pmatrix}. \quad (3.19)$$

For the one-site system, the Eq. (3.15) becomes simplified to

$$\begin{aligned} I_L &= \frac{4e}{h}\Gamma_L^2 \int d\epsilon \mathrm{Tr}\left[D^r \hat{f}_L D^a \tau_3 - D^r \tau_3 \hat{f}_L D^a\right] \\ &+ \frac{4e}{h}\Gamma_L \Gamma_R \int d\epsilon g_2(\epsilon) \mathrm{Tr}\tau_3 \hat{\Omega} \tau_3 \\ &\times \left[D^r \tau_3 \hat{f}_L D^a - D^a \tau_3 f(\epsilon) D^r\right]. \end{aligned} \quad (3.20)$$

Here Γ_p ($p = L, R$) is the linewidth parameter defined by the relation, $\Gamma_p = \pi N_p |V_{p1}|^2$. The first line is the contribution from the Andreev reflection and the second line is the contribution from quasiparticles excited over the superconducting energy gap. The self-energy of a resonant site is given by the equation,

$$\Sigma^r = -i\Gamma_L \mathbf{1} + \Gamma_R g(\epsilon) \tau_3 \hat{\Omega}_R \tau_3, \quad (3.21)$$

$$\Sigma^a = i\Gamma_L \mathbf{1} + \Gamma_R g^*(\epsilon) \tau_3 \hat{\Omega}_R \tau_3. \quad (3.22)$$

Here $\mathbf{1}$ is a 2×2 unit matrix. Inserting the Green's functions of a resonant site, the current can be written in terms of the transmission probability $T(\epsilon)$,

$$I_L = \frac{2e}{h} \int d\epsilon T(\epsilon) \left[f(\epsilon) - f(\epsilon - \mu_L)\right]. \quad (3.23)$$

$T(\epsilon)$ is defined as a sum of two, $T(\epsilon) = T_A(\epsilon) + T_{qp}(\epsilon)$. The Andreev reflection gives

$$\begin{aligned} T_A(\epsilon) &= 8\Gamma_L^2 |D_{12}^r(\epsilon)|^2 \\ &= \frac{8\Gamma_L^2 \Gamma_R^2}{|Z_1(\epsilon)|^2} \frac{\Delta_R^2}{|\epsilon^2 - \Delta_R^2|} = \frac{8\Gamma_L^2 \Gamma_R^2 \Delta_R^2}{\mathcal{D}(\epsilon)}. \end{aligned} \quad (3.24)$$

Here Z_1 is the determinant of $[D^r(\epsilon)]^{-1}$ and the denominator $\mathcal{D}$ is given by the expressions,

$$\begin{aligned} \mathcal{D} &= \left[(\epsilon^2 - E_1^2 - \Gamma_L^2 - \Gamma_R^2)\sqrt{\Delta_R^2 - \epsilon^2} + 2\Gamma_R \epsilon^2\right]^2 \\ &+ 4\Gamma_L^2 \epsilon^2 \left[\Gamma_R + \sqrt{\Delta_R^2 - \epsilon^2}\right]^2, \end{aligned} \quad (3.25)$$

for $|\epsilon| < \Delta_R$ and

$$\begin{aligned} \mathcal{D} &= \left[(\epsilon^2 - E_1^2 - \Gamma_L^2 - \Gamma_R^2)\sqrt{\epsilon^2 - \Delta_R^2} - 2\Gamma_L \Gamma_R |\epsilon|\right]^2 \\ &+ 4\epsilon^2 \left[\Gamma_L \sqrt{\epsilon^2 - \Delta_R^2} + \Gamma_R |\epsilon|\right]^2, \end{aligned} \quad (3.26)$$

for $|\epsilon| > \Delta_R$. Though the detailed forms of $T_A(\epsilon)$ are different depending on the energy range, the Andreev contribution is continuous at $|\epsilon| = \Delta_R$.

$$T_A(0) = \frac{8\Gamma_L^2 \Gamma_R^2}{(E_1^2 + \Gamma_L^2 + \Gamma_R^2)^2}, \quad (3.27)$$

$$T_A(\pm\Delta_R) = \frac{2\Gamma_L^2}{\Gamma_L^2 + \Delta_R^2}. \quad (3.28)$$

Note that T_A at $\epsilon = \pm\Delta_R$ is independent of the energy level position E_1 and is always less than a value of 2. The quasiparticle contribution is given in an explicit form as

$$\begin{aligned} T_{qp}(\epsilon) &= 4\Gamma_L \Gamma_R |g_2(\epsilon)| \left[|\epsilon| \left\{|D_{11}^r(\epsilon)|^2 + |D_{12}^r(\epsilon)|^2\right\} - \Delta_R \mathrm{sgn}(\epsilon) \mathrm{Re}\left\{D_{11}^r(\epsilon) D_{12}^a(\epsilon) - D_{22}^r(-\epsilon) D_{12}^a(-\epsilon)\right\}\right] \\ &= \frac{4\Gamma_L \Gamma_R \sqrt{\epsilon^2 - \Delta_R^2}\left[|\epsilon| \left\{(\epsilon + E_1)^2 + \Gamma_L^2 + \Gamma_R^2\right\} + 2\Gamma_L \Gamma_R \sqrt{\epsilon^2 - \Delta_R^2}\right]}{\left[(\epsilon^2 - E_1^2 - \Gamma_L^2 - \Gamma_R^2)\sqrt{\epsilon^2 - \Delta_R^2} - 2\Gamma_L \Gamma_R |\epsilon|\right]^2 + 4\epsilon^2 \left[\Gamma_L \sqrt{\epsilon^2 - \Delta_R^2} + \Gamma_R |\epsilon|\right]^2}. \end{aligned} \quad (3.29)$$

As expected, the quasiparticle contribution vanishes at $|\epsilon| = \Delta_R$. When the right lead becomes normal or $\Delta_R = 0$, the Andreev contribution vanishes and the quasiparticle contribution is simplified to the well-known Lorentzian form, $T_{qp} = 4\Gamma_L \Gamma_R / [(\epsilon - E_1)^2 + (\Gamma_L + \Gamma_R)^2]$.

C. Atomic wire: serial multi-sites

When multi-sites are arranged in series like atomic wires, the current can be simplified considerably. Since the left (right)-most site is coupled to the left (right) lead, respectively, the coupling matrices to the leads are given by the expressions,

$$V_L^\dagger = \begin{pmatrix} V_{L1} & 0 & \mathbf{0} & \cdots & \mathbf{0} \\ 0 & V_{1L} & & & \end{pmatrix}, \tag{3.30}$$

$$V_R^\dagger = \begin{pmatrix} \mathbf{0} & \cdots & \mathbf{0} & V_{RN} & 0 \\ & & & 0 & V_{NR} \end{pmatrix}. \tag{3.31}$$

Here $\mathbf{0}$ is the 2×2 zero matrix. Various matrices appearing in the expression of current are also simplified. For example,

$$[\pi N_L V_L V_L^\dagger]_{ij} = \Gamma_L \mathbf{1} \delta_{i,1}\delta_{j,1}. \tag{3.32}$$

Here $\mathbf{1}$ is the 2×2 unit matrix in the Nambu spinor space. The Andreev contribution to current can be written in components as

$$\begin{aligned} I_A &= \frac{4e}{h}\int d\epsilon \mathrm{Tr}\left[\mathbf{D}^r_{11}\Gamma_L \hat{f}_L \mathbf{D}^a_{11}\Gamma_L\tau_3 - \mathbf{D}^r_{11}\Gamma_L \hat{f}_L \tau_3 \mathbf{D}^a_{11}\Gamma_L\right] \\ &= \frac{8e}{h}\cdot\Gamma_L^2 \int d\epsilon |D^r_{11,12}(\epsilon)|^2 \left[f(\epsilon+\mu_L) - f(\epsilon-\mu_L)\right] \end{aligned} \tag{3.33}$$

The indices i and j in $D_{ij,\alpha\beta}$ denote the sites of resonant levels while the indices α and β mean the elements of the 2×2 matrix in the Nambu spinor space.

$$\begin{aligned} I_A &= \frac{2e}{h}\int d\epsilon T_A(\epsilon)\left[f(\epsilon) - f(\epsilon-\mu_L)\right], \quad (3.34) \\ T_A(\epsilon) &= 4\Gamma_L^2\left[|D^r_{11,12}(\epsilon)|^2 + |D^r_{11,12}(-\epsilon)|^2\right]. \quad (3.35) \end{aligned}$$

The Andreev conductance is given in a simple form,

$$G_{NS} = 2\cdot\frac{2e^2}{h}\cdot 4\Gamma_L^2 |D^r_{11,12}(0)|^2. \tag{3.36}$$

The quasiparticle contribution to current is also given in components by the equation,

$$\begin{aligned} I_{qp} &= -\frac{4e}{h}\int d\epsilon\ \Gamma_L \overline{\Gamma}_R(\epsilon)\mathrm{sgn}(\epsilon)\mathrm{Tr}\tau_3\hat{\Omega}_R\tau_3 \\ &\quad \times\left[\mathbf{D}^r_{N1}\hat{f}_L\tau_3\mathbf{D}^a_{1N} - \mathbf{D}^a_{N1} f \tau_3 \mathbf{D}^r_{1N}\right]. \end{aligned} \tag{3.37}$$

Here $\overline{\Gamma}_R(\epsilon) = \Gamma_R |g_2(\epsilon)|$. After some algebra, the quasiparticle contribution to the current can be written as

$$\begin{aligned} I_{qp} &= \frac{2e}{h}\int d\epsilon T_{qp}(\epsilon)\left[f(\epsilon) - f(\epsilon-\mu_L)\right], \quad (3.38) \\ T_{qp}(\epsilon) &= 2\Gamma_L\overline{\Gamma}_R(\epsilon)|\epsilon|\left[|D^r_{N1,11}(\epsilon)|^2 + |D^r_{N1,12}(\epsilon)|^2 + |D^r_{N1,22}(-\epsilon)|^2 + |D^r_{N1,12}(-\epsilon)|^2\right] \\ &\quad -4\Gamma_L\overline{\Gamma}_R(\epsilon)\Delta_R\mathrm{sgn}(\epsilon)\ \mathrm{Re}\left[D^r_{N1,11}(\epsilon)D^a_{1N,12}(\epsilon) - D^r_{N1,22}(-\epsilon)D^a_{1N,21}(-\epsilon)\right]. \quad (3.39) \end{aligned}$$

The total transmission probability is a sum of two contributions: $T = T_A + T_{qp}$. Though we are using the word "probability", it is a misnomer because T can become larger than a unity due to the Andreev reflection below the superconducting energy gap.

In a serial multi-site configuration, the retarded self-energy is given by the expression,

$$\Sigma^r_{ij} = -i\Gamma_L\mathbf{1}\delta_{i,1}\delta_{j,1} + \Gamma_R g(\epsilon)\tau_3\hat{\Omega}_R\tau_3\ \delta_{i,N}\delta_{j,N}, \tag{3.40}$$

and the retarded Green's function of multi-site system is expressed by the matrix inversion, $D^r = [\epsilon - H_d - \Sigma^r]^{-1}$. We now calculate the Andreev conductance of multi-site atomic wire one by one. For one resonant site, the Green's function is given by the equation,

$$D^r(\epsilon) = \begin{pmatrix} \epsilon Z_R - E_1 + i\Gamma_L & \Gamma_R\Delta_R g(\epsilon) \\ \Gamma_R\Delta_R g(\epsilon) & \epsilon Z_R + E_1 + i\Gamma_L \end{pmatrix}^{-1} \tag{3,41}$$

$$G_{NS} = 2\cdot\frac{2e^2}{h}\cdot\frac{4\Gamma_L^2\Gamma_R^2}{[E_1^2 + \Gamma_L^2 + \Gamma_R^2]^2}. \tag{3.42}$$

Here $Z_R = 1 - \Gamma_R g(\epsilon)$ and the one-site system is detailed in the previous section. For two-site atomic wire, the Green's function relevant to the Andreev reflection is

$$D^r_{11,12}(\epsilon) = \frac{|t_1|^2\Delta_R\Gamma_R g(\epsilon)}{Z_2(\epsilon)}, \tag{3.43}$$

where

$$\begin{aligned} Z_2(\epsilon) &= [(\epsilon + i\Gamma_L)^2 - E_1^2][\epsilon^2 - E_2^2 - \Gamma_R^2 - 2\epsilon^2\Gamma_R g] \\ &\quad -2|t_1|^2\left[(\epsilon + i\Gamma_L)(\epsilon - \epsilon\Gamma_R g) + E_1 E_2\right] \\ &\quad +|t_1|^4. \end{aligned} \tag{3.44}$$

The Andreev conductance is

$$\begin{aligned} G_{NS} &= 2\cdot\frac{2e^2}{h}\cdot\frac{4\Gamma_L^2\Gamma_R^2|t_1|^4}{|Z_1(0)|^2}, \quad (3.45) \\ Z_2(0) &= (E_1^2 + \Gamma_L^2)(E_2^2 + \Gamma_R^2) + |t_1|^4 \\ &\quad -2|t_1|^2 E_1 E_2. \quad (3.46) \end{aligned}$$

At $\epsilon = \pm\Delta_R$, T_A is independent of E_2 and is given by the expression,

$$T_A = \frac{2\Gamma_L^2 t_1^4}{\Delta_R^2(E_1^2 + \Gamma_L^2 + t_1^2 - \Delta_R^2)^2 + \Gamma_L^2(2\Delta_R^2 - t_1^2)^2} \tag{3.47}$$

T_A at $\epsilon = \pm\Delta_R$ can reach the maximum value of 2 when $E_1 = 0$ and $\Gamma_L = \sqrt{t^2 - \Delta_R^2}$. For three-site atomic wire, the Green's function at the Fermi energy is

$$D^r_{11,12}(0) \;=\; \frac{|t_1|^2|t_2|^2\Gamma_R}{Z_3(0)}, \qquad (3.48)$$

where

$$\begin{aligned} Z_3(0) \;&=\; \det(-\mathbf{H}_d + i\Gamma) \\ &=\; -(E_1^2+\Gamma_L^2)E_2^2(E_3^2+\Gamma_R^2) - |t_2|^4(E_1^2+\Gamma_L^2) \\ &\quad -|t_1|^4(E_3^2+\Gamma_R^2) + 2E_2E_3|t_2|^2(E_1^2+\Gamma_L^2) \\ &\quad +|t_1|^2\left\{E_1E_2(2E_3^2+\Gamma_L^2) - E_1E_3|t_2|^2\right\} \\ &\quad -i|t_1|^2\Gamma_L(E_2\Gamma_L^2 - E_3|t_2|^2). \qquad (3.49) \end{aligned}$$

When $E_i = 0$ for all i's, the Andreev conductance is given in a simple form,

$$\begin{aligned} D^r_{11,12}(0) \;&=\; -\frac{|t_1|^2|t_2|^2\Gamma_R}{\Gamma_L^2|t_2|^4 + \Gamma_R^2|t_1|^4}, \qquad (3.50) \\ G_{NS} \;&=\; 2\cdot\frac{2e^2}{h}\cdot\frac{4\Gamma_L^2|t_2|^4\cdot\Gamma_R^2|t_1|^4}{\left[\Gamma_L^2|t_2|^4 + \Gamma_R^2|t_1|^4\right]^2}. \qquad (3.51) \end{aligned}$$

We can now deduce the general expression of the Andreev conductance for N-site atomic wire. Depending on the parity of the number of atoms in the atomic wire, the Andreev conductance takes different forms,

$$\begin{aligned} G_{NS} \;&=\; \frac{2e^2}{h}\cdot T_N(0), \qquad (3.52) \\ T_1(0) \;&=\; \frac{8\cdot\Gamma_L^2\cdot\Gamma_R^2}{\left[\Gamma_L^2+\Gamma_R^2\right]^2}, \qquad (3.53) \\ T_{2N+1}(0) \;&=\; \frac{8\cdot\Gamma_L^2|t_2t_4\cdots t_{2N}|^4\cdot\Gamma_R^2|t_1t_3\cdots t_{2N-1}|^4}{\left[\Gamma_L^2|t_2t_4\cdots t_{2N}|^4 + \Gamma_R^2|t_1t_3\cdots t_{2N-1}|^4\right]^2}, \qquad (3.54) \\ T_2(0) \;&=\; \frac{8\cdot\Gamma_L^2\Gamma_R^2\cdot|t_1|^4}{\left[\Gamma_L^2\Gamma_R^2+|t_1|^4\right]^2}, \qquad (3.55) \\ T_{2N}(0) \;&=\; \frac{8\cdot\Gamma_L^2|t_2t_4\cdots t_{2N-2}|^4\Gamma_R^2\cdot|t_1t_3\cdots t_{2N-1}|^4}{\left[\Gamma_L^2|t_2t_4\cdots t_{2N-2}|^4\Gamma_R^2 + |t_1t_3\cdots t_{2N-1}|^4\right]^2}. \qquad (3.56) \end{aligned}$$

The even-odd behavior is also evident in the Andreev conductance as in the NAN junction connected by the atomic wire. Since the Andreev reflection is the two-particle process, all the parameters in the transmission probability at E_F in the NAS junction are squared compared to the NAN junction. In the mirror symmetric atomic wire, $T_{2N+1}(0)$ does not depend on the detailed values of the hopping matrices in the atomic chain but is determined by the couplings to the leads.

$$T_{2N+1}(0) \;=\; \frac{8\cdot\Gamma_L^2\cdot\Gamma_R^2}{\left[\Gamma_L^2+\Gamma_R^2\right]^2}. \qquad (3.57)$$

$T_{2N}(0)$ depends on the hopping matrices in the atomic wire. When all the hopping integrals are equal (a special case of the mirror symmetric chain), the transmission probability at the Fermi energy is simplified as

$$\begin{aligned} T_{2N+1}(0) \;&=\; \frac{8\cdot\Gamma_L^2\cdot\Gamma_R^2}{\left[\Gamma_L^2+\Gamma_R^2\right]^2}, \qquad (3.58) \\ T_{2N}(0) \;&=\; \frac{8\cdot\Gamma_L^2\Gamma_R^2\cdot t^4}{\left[\Gamma_L^2\Gamma_R^2+t^4\right]^2}. \qquad (3.59) \end{aligned}$$

The maximum transmission is achieved when $\Gamma_L = \Gamma_R$ in the odd-numbered atomic wire, and when $t^2 = \Gamma_L\Gamma_R$ in the even-numbered atomic wire.

To illustrate the even-odd parity dependence of the transmission probability $T_N(\epsilon) = T_A(\epsilon) + T_{qp}(\epsilon)$, we plot $T_N(\epsilon)$ for differing N's (see Figs. 6 and 7). The model parameters are chosen as follows: $E_i = 0$ for all the sites and $t_i = t$ for all i's. The superconducting energy gap $\Delta_R = t/10$ is chosen to be large to show clearly the Andreev structure in $T_N(\epsilon)$. The results for the case $\Gamma_{L,R} = 0.3\times t$ are displayed in Fig. 6. Note that the Andreev contribution of $T_A(\epsilon)$ is appreciable only inside the superconducting energy gap. For odd-numbered atomic wires, the transmission probability displays the Andreev peak at the Fermi energy and the side peaks above the superconducting energy gap which are the quasiparticle contributions. For even-numbered atomic wires, the transmission probability is suppressed at the Fermi energy and is peaked at the superconducting energy gap. Other peaks outside the superconducting energy gap are contributions from the quasiparticles.

When the coupling to the leads is larger than the hopping integral in the atomic wire, the spectral shape of $T_N(\epsilon)$ is different compared to the case of $\Gamma_{L,R} < t$. The results of $T_N(\epsilon)$ when $\Gamma_{L,R} = 1.2\times t$ are displayed in Fig. 7. Increased coupling to the leads results in a broadened spectral shape of the transmission probability. In the odd-numbered atomic wire, the transmission probability is almost flat inside the superconducting gap. In the even-numbered atomic wire, the Andreev conductance is increased as $\Gamma_{L,R}$ is increased($t > \sqrt{\Gamma_L\Gamma_R}$), reaches the maximum value of 2 when $t = \sqrt{\Gamma_L\Gamma_R}$ and is decreased with further increasing $\Gamma_{L,R}$($\sqrt{\Gamma_L\Gamma_R} > t$).

The local DOS at each atomic site in the atomic wire is computed and displayed in Figs. 8 and 9. The shape of local DOS is dependent on the parity of the number of atoms in the atomic wire. The local DOS also depends on the atom's position in the chain.

IV. SUMMARY AND CONCLUSION

Using the tight-binding Hamiltonian, we studied the dependence of the conductance and shot noise on the number of atoms in the atomic wire when the atomic wire is connected to the two metallic leads or to the metal and superconducting leads. In metal-atomic wire-metal(NAN) junctions, the even-odd parity dependence of the conductance can be understood by the energy-level splitting in quantum physics and the particle-hole symmetry of atomic energy levels. The linear response conductance is larger in the odd-numbered atomic wire than in the even-numbered atomic wire. The conductance can reach the maximum possible value $2e^2/h$ in the odd-numbered atomic wire when all the atomic energy levels lie at the Fermi energy (resonance condition) and the system is mirror symmetric with respect to the center of the wire. The shot noise also displays the even-odd parity effects depending on the number of atoms in the atomic wire. In contrast to the conductance, the shot noise is larger in the even-numbered atomic wire than in the odd-numbered atomic wire.

We also studied the Andreev conductance in the metal-atomic wire-superconducting junctions. As in the NAN junctions, the Andreev conductance displays the even-odd parity effects. In the odd-numbered atomic wire, the conductance is enhanced and close to $4e^2/h$ due to the Andreev reflection. The maximum Andreev conductance $4e^2/h$ is possible in the mirror-symmetric odd-numbered atomic wire when the resonance condition is satisfied. On the other hand, the conductance is suppressed below $4e^2/h$ in the even-numbered atomic wire even when the resonance condition is satisfied for the mirror-symmetric case.

Acknowledgments

We would like to thank H. W. Lee for his careful reading of this manuscript. This work was supported in part by the National Science Foundation under Grant No. DMR 9357474, in part by the BK21 project and in part by grant No. 1999-2-114-005-5 from the KOSEF.

APPENDIX A: DERIVATION OF EQ. (2.17)

In this Appendix, we find the expression of the current noise by calculating the Feynman diagrams shown in Fig. 2. We calculate each diagram step by step. The diagram in Fig. 2(a) gives

$$i\hbar G_{II}(t,t') = -\frac{e^2}{V^2}\sum_{kk'}\int_C dt_1 \int_C dt_2 \ \mathrm{Tr}\left\{D(t,t_1)V_L G_{cL}(k';t_1,t')V_L^\dagger D(t',t_2)V_L G_{cL}(k;t_2,t)V_L^\dagger\right\}. \tag{A1}$$

After some algebra, the lesser part is given by the equation

$$\hbar G_{II}^<(\epsilon) = \frac{e^2}{h}\int d\zeta \ \mathrm{Tr}\left\{\left[iD^<(\epsilon+\zeta)+2f_L(\epsilon+\zeta)D^r(\epsilon+\zeta)\right]\Gamma_L\left[iD^>(\zeta)+2\bar{f}_L(\zeta)D^r(\zeta)\right]\Gamma_L\right\}. \tag{A2}$$

We use the analytic continuation to the real-time axis[14] to find the lesser current Green's function. The diagram in Fig. 2(b) gives

$$i\hbar G_{II}(t,t') = -\frac{e^2}{V^2}\sum_{kk'}\int_C dt_1 \int_C dt_2 \ \mathrm{Tr}\left\{V_L G_{cL}(k;t,t_1)V_L^\dagger D(t_1,t')V_L G_{cL}(k';t',t_2)V_L^\dagger D(t_2,t)\right\}, \tag{A3}$$

$$\hbar G_{II}^<(\epsilon) = \frac{e^2}{h}\int d\zeta \ \mathrm{Tr}\left\{\Gamma_L\left[-iD^<(\epsilon+\zeta)+2f_L(\epsilon+\zeta)D^a(\epsilon+\zeta)\right]\Gamma_L\left[-iD^>(\zeta)+2\bar{f}_L(\zeta)D^a(\zeta)\right]\right\}. \tag{A4}$$

Two diagrams in Fig. 2(c) give

$$\begin{aligned} i\hbar G_{II}(t,t') &= \frac{e^2}{V}\sum_{k}\mathrm{Tr}\left\{V_L G_{cL}(k;t,t')V_L^\dagger D(t',t)\right\} \\ &\quad +\frac{e^2}{V^2}\sum_{kk'}\int_C dt_1 \int_C dt_2 \ \mathrm{Tr}\left\{V_L G_{cL}(k;t,t_2)V_L^\dagger D(t_2,t_1)V_L G_{cL}(k';t_1,t')V_L^\dagger D(t',t)\right\}, \end{aligned} \tag{A5}$$

$$\begin{aligned} \hbar G_{II}^<(\epsilon) &= -\frac{2e^2}{h}\int d\zeta \ f_L(\epsilon+\zeta)\mathrm{Tr}\{\Gamma_L D^>(\zeta)\} \\ &\quad -\frac{e^2}{h}\int d\zeta \ \mathrm{Tr}\left\{\Gamma_L\left[D^<(\epsilon+\zeta)+2if_L(\epsilon+\zeta)\{D^a(\epsilon+\zeta)-D^r(\epsilon+\zeta)\}\right]\Gamma_L D^>(\zeta)\right\}. \end{aligned} \tag{A6}$$

Two diagrams in Fig. 2(d) give

$$\begin{aligned}
i\hbar G_{II}(t,t') &= \frac{e^2}{V}\sum_k \mathrm{Tr}\left\{D(t,t')V_L G_{cL}(k;t',t)V_L^\dagger\right\} \\
&+\frac{e^2}{V^2}\sum_{kk'}\int_C dt_1\int_C dt_2\ \mathrm{Tr}\left\{D(t,t')V_L G_{cL}(k';t',t_2)V_L^\dagger D(t_2,t_1)V_L G_{cL}(k;t_1,t)V_L^\dagger\right\}, \qquad \text{(A7)}\\
\hbar G^<_{II}(\epsilon) &= -\frac{2e^2}{h}\int d\zeta\ \bar{f}_L(\zeta)\mathrm{Tr}\{D^<(\epsilon+\zeta)\Gamma_L\} \\
&-\frac{e^2}{h}\int d\zeta\ \mathrm{Tr}\left\{D^<(\epsilon+\zeta)\Gamma_L\left[D^>(\zeta)+2i\bar{f}_L(\zeta)\{D^a(\zeta)-D^r(\zeta)\}\right]\Gamma_L\right\}. \qquad \text{(A8)}
\end{aligned}$$

Collecting all contributions, the lesser current Green's function is given by the expression,

$$\begin{aligned}
\hbar G^<_{II}(\epsilon) &= \frac{e^2}{h}\int d\zeta \mathrm{Tr}[2f_L(\epsilon+\zeta)D^r(\epsilon+\zeta)+iD^<(\epsilon+\zeta)]\Gamma_L[2\bar{f}_L(\zeta)D^r(\zeta)+iD^>(\zeta)]\Gamma_L \\
&+\frac{e^2}{h}\int d\zeta \mathrm{Tr}[2f_L(\epsilon+\zeta)D^a(\epsilon+\zeta)-iD^<(\epsilon+\zeta)]\Gamma_L[2\bar{f}_L(\zeta)D^a(\zeta)-iD^>(\zeta)]\Gamma_L \\
&-\frac{2e^2}{h}\int d\zeta\ f_L(\epsilon+\zeta)\mathrm{Tr}\{\Gamma_L D^>(\zeta)\} \\
&-\frac{e^2}{h}\int d\zeta\ \mathrm{Tr}\left\{\Gamma_L\left[D^<(\epsilon+\zeta)+2if_L(\epsilon+\zeta)\{D^a(\epsilon+\zeta)-D^r(\epsilon+\zeta)\}\right]\Gamma_L D^>(\zeta)\right\} \\
&-\frac{2e^2}{h}\int d\zeta\ \bar{f}_L(\zeta)\mathrm{Tr}\{D^<(\epsilon+\zeta)\Gamma_L\} \\
&-\frac{e^2}{h}\int d\zeta\ \mathrm{Tr}\left\{D^<(\epsilon+\zeta)\Gamma_L\left[D^>(\zeta)+2i\bar{f}_L(\zeta)\{D^a(\zeta)-D^r(\zeta)\}\right]\Gamma_L\right\}. \qquad \text{(A9)}
\end{aligned}$$

The current noise is then given by $S(\epsilon) = -\hbar G^<_{II}(\epsilon) - \hbar G^<_{II}(-\epsilon)$. In particular, the $\omega = 0$ component current noise $S_0 = -2\hbar G^<_{II}(0)$ is given by the equation,

$$\begin{aligned}
S_0 &= \frac{8e^2}{h}\int d\epsilon\ \mathrm{Tr}\Gamma_L D^<\Gamma_L D^> \\
&-\frac{8e^2}{h}\int d\epsilon\ f_L\bar{f}_L\mathrm{Tr}\Gamma_L[D^r\Gamma_L D^r + D^a\Gamma_L D^a] \\
&-\frac{8e^2}{h}\int d\epsilon\ f_L\mathrm{Tr}\Gamma_L D^>\Gamma_L\cdot i[D^r-D^a] \\
&-\frac{8e^2}{h}\int d\epsilon\ \bar{f}_L\mathrm{Tr}\Gamma_L D^<\Gamma_L\cdot i[D^r-D^a] \\
&+\frac{4e^2}{h}\int d\epsilon\ \left[f_L\mathrm{Tr}\Gamma_L D^> + \bar{f}_L\mathrm{Tr}\Gamma_L D^<\right]. \qquad \text{(A10)}
\end{aligned}$$

The above expression of S_0 looks highly asymmetrical in the indices of left and right leads or L and R. Substituting the following identity relations

$$\begin{aligned}
D^{<,>} &= D^r\Sigma^{<,>}D^a, && \text{(A11)}\\
\Sigma^< &= 2f_L\Gamma_L + 2f_R\Gamma_R, && \text{(A12)}\\
\Sigma^> &= 2\bar{f}_L\Gamma_L + 2\bar{f}_R\Gamma_R, && \text{(A13)}\\
i[D^r-D^a] &= 2D^r\Gamma D^a, && \text{(A14)}
\end{aligned}$$

we simplify the expression of current noise S_0 as

$$\begin{aligned}
S_0 &= \frac{2e^2}{h}\int d\epsilon[f_L\bar{f}_L + f_R\bar{f}_R]\mathrm{Tr}\mathbf{T}^2 \\
&+\frac{2e^2}{h}\int d\epsilon[f_L\bar{f}_R + \bar{f}_L f_R]\left[\mathrm{Tr}\mathbf{T} - \mathrm{Tr}\mathbf{T}^2\right] \qquad \text{(A15)}
\end{aligned}$$

Here $\mathbf{T} \equiv 4\Gamma_L D^r\Gamma_R D^a$.

APPENDIX B: PROPERTIES OF DETERMINANT $Z_N(\epsilon)$: EQ. (2.26)

In this Appendix, we study the properties of the determinant $Z_N(\epsilon)$ which is defined by the Eq. (2.26). We can readily find the iterative relation for the determinant when $\Gamma_{L,R} = 0$ and $E_i = 0$ for all i's,

$$\begin{aligned}
Z_{N+2}(\epsilon) &= \epsilon Z_{N+1}(\epsilon) - |t_{N+1}|^2 Z_N(\epsilon), && \text{(B1)}\\
Z_2(\epsilon) &= \epsilon^2 - |t_1|^2, && \text{(B2)}\\
Z_3(\epsilon) &= \epsilon(\epsilon^2 - |t_1|^2 - |t_2|^2). && \text{(B3)}
\end{aligned}$$

Especially when $t_i = t$ for all i's, the expression of $Z_N(\epsilon)$ can be found in an explicit form,

$$Z_N(\epsilon) = \prod_{k=1}^{N}\left[\epsilon - 2|t|\cos\frac{k\pi}{N+1}\right]. \qquad \text{(B4)}$$

$Z_N(\epsilon)$ is the type-II Chebyshev polynomial.

From the recursive relation, we can deduce that $Z_N(\epsilon)$ is invariant under the transformation, $t_i \to -t_i$ for any i. We can also show from the recursive relation that $Z_N(\epsilon)$ satisfies the parity relation: $Z_N(-\epsilon) = (-1)^N Z_N(\epsilon)$. This parity relation has the important consequence on the particle-hole symmetry of split atomic energy level structure. $Z_{2N}(\epsilon)$ is the even function of ϵ and $Z_{2N}(0) = (-1)^N |t_1 t_3 \cdots t_{2N-1}|^2$. $Z_{2N+1}(\epsilon)$ can be written as $Z_{2N+1}(\epsilon) = \epsilon Y_{2N+1}(\epsilon)$ where $Y_{2N+1}(\epsilon)$ is the even function of ϵ and $Y_{2N+1}(0) \neq 0$. When all the atomic energy levels lie at the Fermi energy, the hopping integrals between neighboring sites in the atomic wire lift the degeneracy but does not change the particle-hole symmetry of split energy levels. If ϵ_0 is a solution of $Z_N(\epsilon) = 0$, so is $-\epsilon_0$ because of the parity relation. Since $Z_N(0) \neq 0$ for even N, no split levels lie at the Fermi energy. Since $Z_N(0) = 0$ for odd N, $\epsilon = 0$ is a solution of the secular equation $Z_N(\epsilon) = 0$. Since $Y_N(0) \neq 0$ for odd N, only one level lies at the Fermi energy for the odd-numbered atomic wire.

Though the particle-hole symmetry of split atomic energy levels is shown explicitly, it can be also proved by noting that the tight-binding Hamiltonian is invariant under the particle-hole transformation: $c_i \to (-1)^i c_i^\dagger$. Obviously the Hamiltonian $H = \sum_i (t_i c_{i+1}^\dagger c_i + H.c.)$ remains invariant under this particle-hole transformation.

---

[1] A. I. Yanson, G. R. Bollinger, H. E. van den Brom, N. Agrait, and J. M. van Ruitenbeck, Nature **395**, 783 (1998).

[2] H. Ohnishi, Y. Kondo, and K. Takayanagi, Nature **395**, 780 (1998).

[3] J. M. Krans, C. J. Muller, I. K. Yanson, Th. C. M. Govaert, R. Hesper and J. M. van Ruitenbeek, Phys. Rev. B **48**, 14721 (1993).

[4] F. R. Waugh, M. J. Berry, D. J. Mar, R. M. Westervelt, K. L. Campman and A. C. Gossard, Phys. Rev. Lett. **75**, 705 (1995).

[5] G. Rubio-Bollinger, S. R. Bahn, N. Agrait, K. W. Jacobsen, and S. Vieira, Phys. Rev. Lett. **87**, 026101 (2001).

[6] N. D. Lang and Ph. Avouris, Phys. Rev. Lett. **81**, 3515 (1998); *ibid* **84**, 358 (2000).

[7] H.-S. Sim, H.-W. Lee and K. J. Chang, Phys. Rev. Lett. **87**, 096803 (2001).

[8] P. L. Pernas, A. Martin-Rodero, and F. Flores, Phys. Rev. B **41**, 8553 (1990).

[9] Z. Y. Zeng and F. Claro, cond-mat/0110057.

[10] R. Landauer, IBM J. Res. Dev. **1**, 233 (1957).

[11] M. Büttiker, Phys. Rev. Lett. **57**, 1761 (1986).

[12] G.B. Lesovik, Pis'ma Zh. Éksp. Teor. Fiz. **49**, 513 (1989) [JETP Lett. **49**, 592(1989)]; Also look at the review article, Ya. M. Blanter and M. Büttiker, Physics Reports **336**, 1 (2000).

[13] L.V. Keldysh, Zh. Éksp. Teor. Fiz. **47**, 1515 (1964). [Sov. Phys. JETP **20**, 1018 (1965)]

[14] D.C. Langreth, 1976, in *Linear and Nonlinear Electron Transport in Solids*, Vol.**17** of *NATO Advanced Study Institute, Series B: Physics*, edited by J.T. Devreese and V.E. van Doren (Plenum, New York, 1976), p. 3.

[15] T. V. Shahbazyan and M. E. Raikh, Phys. Rev. B **49**, 17123 (1994).

[16] A. L. Yeyati, A. Martin-Rodero and F. Flores, Phys. Rev. B **56**, 10369 (2001).

[17] J. Friedel, Can. J. Phys. **34**, 1190 (1956).

[18] A. F. Andreev, Zh. Éksp. Teor. Fiz. **46**, 1823 (1964) [Sov. Phys. JETP **19**, 1228 (1964)]; **49**, 655 (1966) [**22**, 455 (1966)].

[19] A. Oguri, Phys. Rev. B **59**, 12240 (1999).

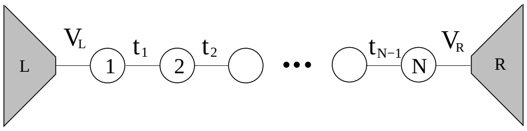

FIG. 1: Schematic display of a serial multi-site system.

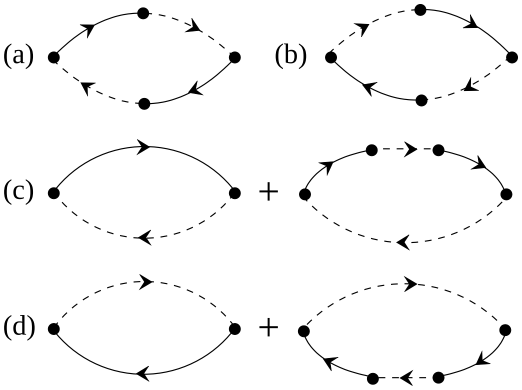

FIG. 2: Feynman diagrams for the current noise. Solid line represents the conduction electron Green's function, while the dashed line means the fully dressed Green's function of the multi-site system.

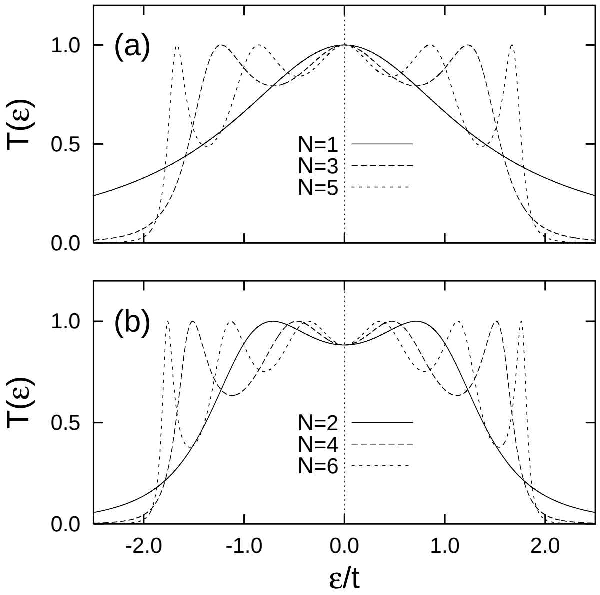

FIG. 3: Dependence of the transmission probability on the number of atoms in atomic wires in the metal-atomic wire-metal junctions. Panel (a) displays the transmission probability for the odd-numbered atomic wires. $T(\epsilon)$ is peaked at the Fermi energy. On the other hand, panel (b) shows the transmission probability for the even-numbered atomic wires. $T(\epsilon)$ is suppressed at the Fermi energy. We take the model parameters: $E_i = 0$ and $t_i = t$ for all sites, $\Gamma_{L,R} = 0.7 \times t$. See the text for explanations.

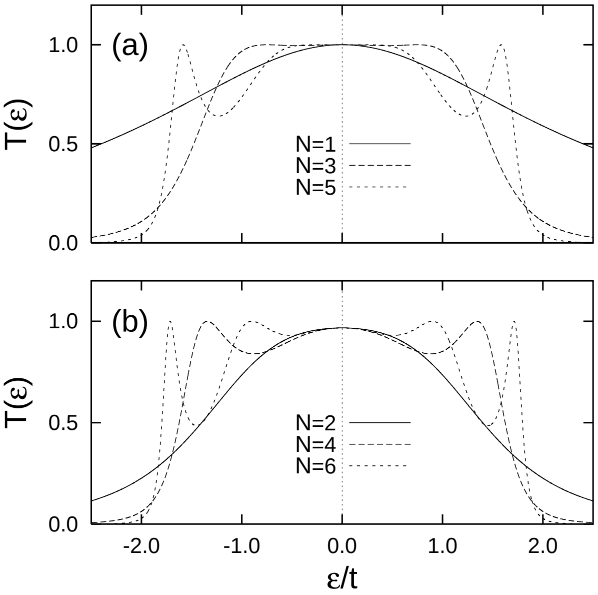

FIG. 4: The transmission probability for blunt tips. Model parameters are the same as in Fig. 3 except for $\Gamma_{L,R} = 1.2\times t$. Increased coupling to the leads broadens the lineshape of the transmission probability. $T_{2N}(\epsilon)$ is peaked at $\epsilon = 0$ when $\Gamma_{L,R} \geq t$.

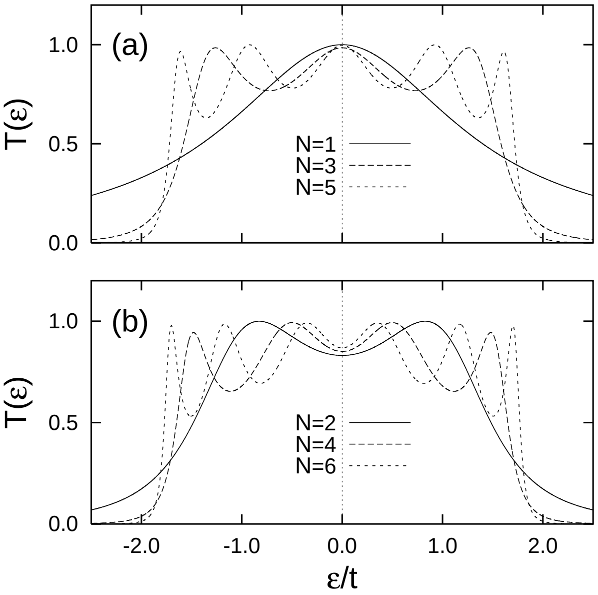

FIG. 5: The transmission probability for disordered hopping matrices. Model parameters are the same as in Fig. 3 except that some disorder in t_i's is introduced: $t_i = t(1 + \delta_i)$ with $|\delta_i| \leq 0.2$.

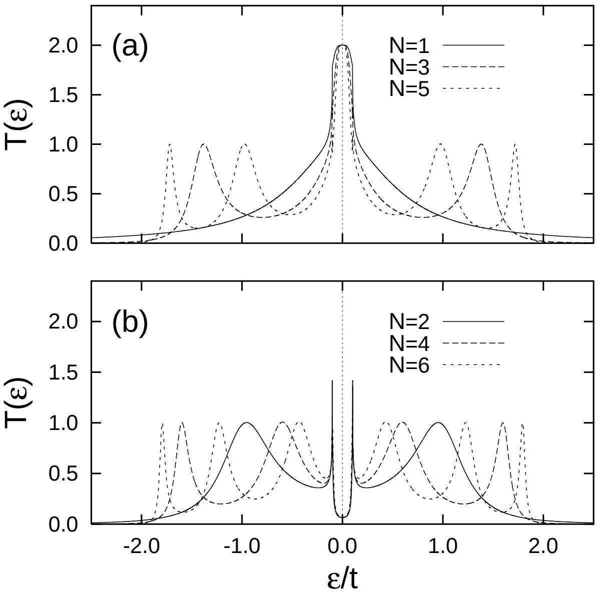

FIG. 6: Dependence of the transmission probability on the number of atoms in an atomic wire in the metal-atomic wire-superconducting junctions. Panel (a) for the odd-numbered atomic wires and panel (b) for the even-numbered atomic wires. We take model parameters: $E_i = 0$ and $t_i = t$ for all sites, $\Gamma_{L,R} = 0.3 \times t$ and the superconducting energy gap $\Delta_R = 0.1 \times t$.

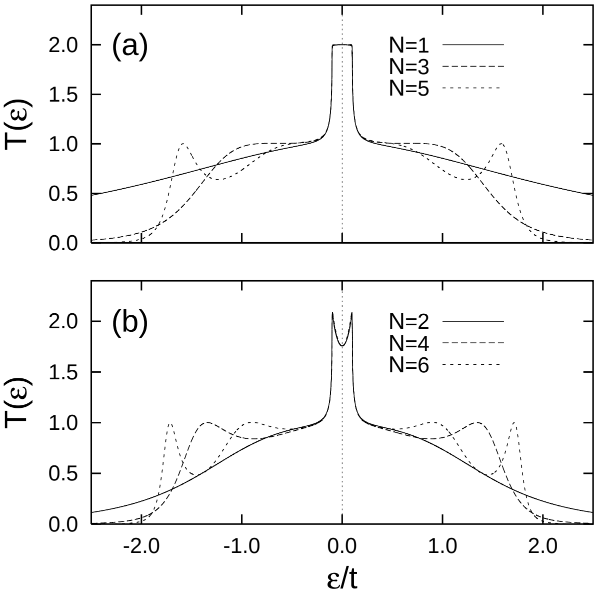

FIG. 7: Dependence of the transmission probability on the number of atoms in an atomic wire in the metal-atomic wire-superconducting junctions. Panel (a) for the odd-numbered atomic wires and panel (b) for the even-numbered atomic wires. We take model parameters: $E_i = 0$ and $t_i = t$ for all sites, $\Gamma_{L,R} = 1.2 \times t$ and the superconducting energy gap $\Delta_R = 0.1 \times t$.

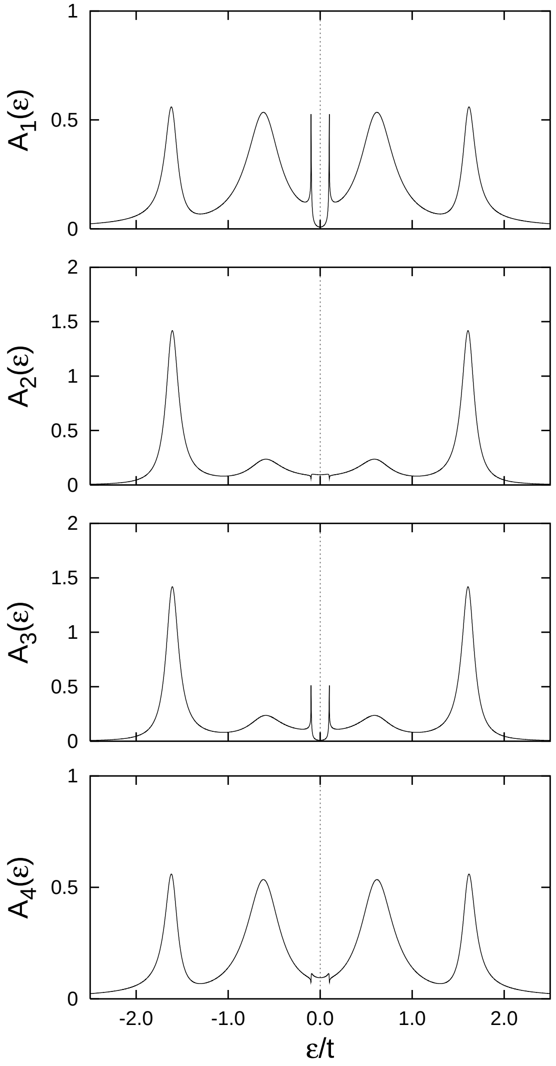

FIG. 8: Local DOS at each atomic site for 4-site atomic wire. A_i means the spectral function of the i-th atoms from the left lead (normal metals). Model parameters are the same as in Fig. 6.

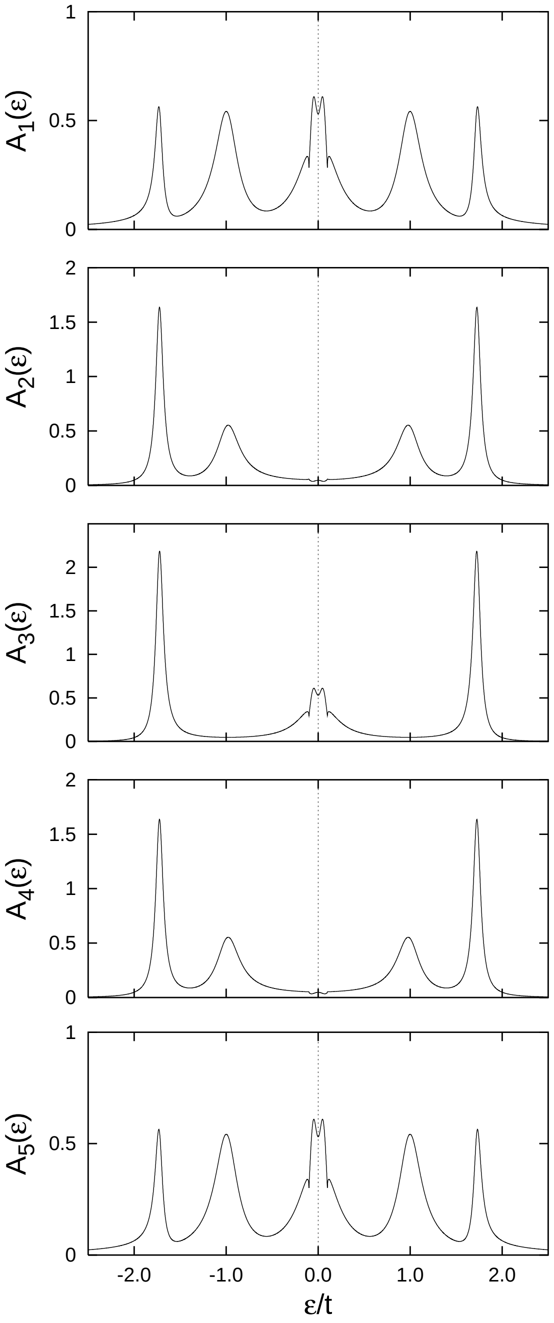

FIG. 9: Local DOS at each atomic site for 5-site atomic wire. A_i means the spectral function of the i-th atoms from the left lead (normal metals). Model parameters are the same as in Fig. 6.